Clays and Clay Minerals, Vol. 64, No. 5, 537–551, 2016.

SURFACE CRYSTAL CHEMISTRY OF PHYLLOSILICATES USING X-RAY PHOTOELECTRON SPECTROSCOPY: A REVIEW

CHIARA ELMI[1,*], STEPHEN GUGGENHEIM[2], AND RETO GIERÉ[1]

[1]Department of Earth and Environmental Science, University of Pennsylvania, 240 S. 33rd Street, Philadelphia, PA 19104-6313, USA

[2]Department of Earth and Environmental Sciences, University of Illinois at Chicago, 845 West Taylor Street, Chicago, IL 60607-7059, USA

Abstract—The characterization of freshly cleaved mica surfaces for surface structure and chemical composition was briefly reviewed and focused on surface crystal chemistry using X-ray photoelectron spectroscopy (XPS) and other surface-sensitive techniques. This paper considers micas, which are useful as a first approximation for the behavior of many clay surfaces. Emphasis was given to phyllosilicate XPS binding energies ("chemical shift"), which were described and used to obtain oxidation state, layer charge, and chemical bonding information from the chemical shifts of different peaks. The chemical shift of the Si_{2p} binding-energy to lower values can result from a negative charge increase because of Si^{4+} replacement by Al^{3+} and/or Fe^{3+}. The apparent interlayer coordination number reduction from twelve to eight at muscovite and tetraferri-phlogopite (001) surfaces was indicated by the XPS measured K_{2p} binding-energy and is consistent with bond relaxation. Although chemical shifts are valuable to distinguish chemical bonding and oxidation state, chemical shifts usually cannot distinguish between different Al coordination environments where Al is in both tetrahedral and octahedral sites.

Key Words—Phyllosilicates, Surface Crystal Chemistry, Surface Structure, XPS.

INTRODUCTION

Interest in mineral surface science has increased significantly over the last decades. Innovative research on mineral surfaces has generated a better understanding of environmentally related aspects and promising industrial process applications. In addition, a better characterization and understanding of Earth material surface properties has been of fundamental importance to mineralogy, geochemistry, solid-state physics, biology, chemistry, and material science, as well as for pharmaceutical and cosmetic applications (Hochella, 1990, 1995; Seyama and Soma, 2003; Carretero and Pozo, 2009, 2010; Maurice, 2009; Somorjai and Li, 2011).

Surfaces of phyllosilicates affect the chemical composition of ground and surface waters through adsorption and desorption of organic and inorganic compounds and by retarding transport of radionuclides and heavy-metal pollutants. These surfaces are also important in rock weathering, soil formation, and oil-field reservoir behavior. The direct study of clay particle surfaces is both difficult and complex because the particles are fine-grained. In contrast, large mica flakes are more easily investigated, and it is generally agreed that micas are useful as a first approximation for the behavior of many clay surfaces (*e.g.* Stucki *et al.*, 1976).

Mineral properties, especially those of layer silicates, depend to a large extent on the arrangement of the atomic planes close to the surface, which may differ from the bulk structure, *e.g.* in regard to redox state, atomic coordination, or chemical bond type. The influence of surface structure on physical properties was demonstrated, for example, by the production of mica-based pearlescent pigments with a parallel alignment of mica particles (Maisch *et al.*, 1996; Gershenkop *et al.*, 2001; Junru *et al.*, 2002; Tenório Cavalcante *et al.*, 2007).

Despite extensive phyllosilicate use in several industrial processes, only limited studies have been conducted to characterize the surface crystal chemistry of freshly cleaved minerals (*i.e.*, Bhattacharyya, 1993; Biino and Groning, 1998; Kuwahara, 1999, 2001; Ilton *et al.*, 2000; Elmi *et al.*, 2013, 2014a, 2014b).

Several studies focused on mechanisms for the cohesion between mica surfaces (Obreimoff, 1930; Gutshall *et al.*, 1970; Metsik, 1972; Giese, 1974; Chan and Richmond, 1977; Christenson, 1993; Moore and Lockner, 2004; Fu *et al.*, 2011; Sakuma, 2013), on weathering (Bancroft *et al.*, 1979; Hochella, 1995; Maurice, 2009), and on metal adsoption between (001) phyllosilicate surfaces and aqueous solutions (Fenter and Sturchio, 2004; Lee *et al.*, 2010, 2012, 2013).

The phyllosilicates are ideal for studying the cohesion between clean, atomically smooth surfaces. Surface properties and, in particular, the arrangement and reactivity of intercalated species in phyllosilicates are influenced by the net negative layer charge, the composition of each surface site, and the topology of the polyhedral linkages (Gutshall *et al.*, 1970; Metsik, 1972; Giese, 1974, 1977, 1978). The origin of layer

* E-mail address of corresponding author:
chiarael@sas.upenn.edu
DOI: 10.1346/CCMN.2016.064033

charge is in isomorphous cation replacement. Layer charge is generally determined by chemical methods, such as the structural-formula method, cation exchange capacity (CEC), and alkylammonium-exchange method (Czímerováa *et al.*, 2006). Adsorbed ions change the phyllosilicate (001) surface negative charge and affect phyllosilicate stability under aqueous conditions (Fenter and Sturchio, 2004; Lee *et al.*, 2010, 2012, 2013). The structure of the interface between muscovite (001) surfaces and aqueous monovalent and divalent metal cation solutions can be measured using *in situ* specular X-ray reflectivity and element-specific resonant anomalous X-ray reflectivity (RAXR) (Lee *et al.*, 2010, 2012, 2013). The charge distribution in each sheet, however, is difficult to establish using X-ray diffraction methods because the unit cell is the average of all structural environments. Complementary to RAXR, X-ray absorption near edge structure (XANES) and extended X-ray absorption fine structure (EXAFS) can provide information on local structures (*i.e.*, Marcelli *et al.*, 2006), adsorbed metal cations (*i.e.*, Beaulieu and Savage, 2005), or dissolution (*i.e.* Show *et al.*, 2009) at the phyllosilicate-water interface.

X-ray photoelectron spectroscopy (XPS) is a useful technique for the analysis of layered structures, such as phyllosilicates, where preferred crystal orientation is achieved easily. XPS is especially valuable for phyllosilicate surface layer charge measurements. This review focuses on the surface structure and chemistry of freshly cleaved phyllosilicates studied using X-ray photoelectron spectroscopy (XPS). The progress obtained in the last decades to clarify structural aspects of freshly cleaved phyllosilicate surfaces is emphasized. In addition, XPS data were compared to results obtained using other surface-sensitive techniques, such as low-energy electron diffraction (LEED), atomic force microscopy (AFM), secondary ion mass spectrometry (SIMS), Auger electron spectrometry (AES), and X-ray photoelectron diffraction (XPD). Starting from the layer silicate bulk structure, where the three-dimensional structure is well established (for a review, see Brigatti and Guggenheim, 2002; Brigatti *et al.*, 2011; Guggenheim, 2011), the present paper considers compositional and structural aspects of freshly cleaved phyllosilicate surfaces. Phyllosilicate XPS binding energies are described here to obtain oxidation state, layer charge, and chemical bonding information from the chemical shifts of different peaks.

The study of phyllosilicates by XPS can potentially be applied in forensic science to identify, for example, thin mineral layers deposited on substrates. These deposits can result from explosions and/or fire, soil and sand traces, particulate matter, cosmetics, or from sequestration of marker elements and molecules on surfaces (Watts, 2010). XPS reveals differences in chemical composition between the surface and the bulk mineral and assesses changes in composition and chemical bonding as a result of surface interactions with other materials. XPS can monitor adsorption, desorption, dissolution, and exchange reactions on mineral surfaces. However, XPS is still not widely used in mineralogy and related geoscience fields to examine crystal chemical variations (*i.e.* cation distribution and replacement, and relaxation or reconstruction effects) from the bulk to the surface.

DESIGN TECHNIQUE FOR PHYLLOSILICATE ANALYSIS

X-ray photoelectron spectroscopy

X-ray photoelectron spectroscopy (XPS), also known as Electron Spectroscopy for Chemical Analysis (ESCA), is a surface-sensitive technique, which determines the concentration and chemical states of elements in the very near-surface layer (1−10 nm) of both conductive and non-conductive materials. All elements, except for H and He, are detectable by XPS at concentrations of >0.1 atomic percent. An added advantage is that XPS is essentially nondestructive even for materials of high susceptibility to damage, such as phyllosilicates. Thus, characteristic features of XPS can reveal differences between the surface and bulk mineral in chemical composition, oxidation state, coordination number, and local bonding environment. In addition, XPS can determine changes in composition and chemical bonding that result from surface interactions with other materials (Seyama *et al.*, 2006). This is possible because the X-radiation commonly used does not produce chemical changes in the surface layers (Wagner *et al.*, 1979).

Surface analysis by XPS is generally performed by sample irradiation using photons under ultra-high vacuum (10^{-8} Torr) using soft X-rays (AlKα at 1486.6 eV or MgKα at 1253.6 eV). The irradiated atoms emit photoelectrons after direct energy transfer from the incident photons to core-level electrons in the target surface. Photoelectrons emitted from atoms near the surface escape into the vacuum chamber, where the electrons are separated according to energy and counted. The photoelectron binding energies are equal to the energy difference between incident photons and the sum of the photoelectron kinetic energy and the work function of the sample-spectrometer system (Kerkhof and Moulijn, 1979; Ratner and Castner, 2009). The binding energy is characteristic of a given energy level for each atom, and thus is dependent on the chemical environment about a given atom (Ratner and Castner, 2009). Therefore, the interpretation of ESCA spectra of phyllosilicate surfaces can provide information on the molecular environment (*i.e.* oxidation state, multiplet structure, chemical bonding, *etc.*) and provide a quantitative elemental analysis of the surface (error < ± 10 %).

Adventitious carbon (*i.e.* aliphatic hydrocarbon), which is ubiquitous, has a 1s-valence band, and this

https://doi.org/10.1346/CCMN.2016.064033 Published online by Cambridge University Press

peak is commonly used to fix the binding-energy scale (assumed C_{1s}-binding energy: 284.8 eV), although this peak has a limited degree of accuracy and precision. Koppelman *et al.* (1980) reported an accuracy of ±0.2 eV and a precision of ±0.1 eV for the C_{1s}-binding energy referenced to the Au_{4f} peak. For micas and phyllosilicates, many authors (Biino and Groning, 1998; Seyama *et al.*, 2006; Elmi *et al.*, 2013, 2014a, 2014b) have shown that repeated analysis of the same spot on a mica sample yielded a precision of ±0.1 eV for C_{1s} when referenced to the Si_{2p} peak. The electron energy shift (peak position) relative to that of the reference compound is termed the chemical shift. The chemical shift of the photoelectron binding energy is dependent on the chemical environment of the atom, in particular the oxidation state. Other local bonding arrangements, including structural relaxation, perhaps can be determined, but results may be complicated by the cleavage process during sample preparation. Because phyllosilicates are insulators, positive electrostatic charges can form at the sample surface due to electron emission during measurement (Seyama *et al.*, 2006). However, the electrical charge on the phyllosilicate surfaces produced during analysis can be neutralized with an electron flood gun.

Angle-resolved XPS (AR-XPS) is a technique that varies the emission angle at which the electrons are collected, thereby enabling electron detection from different depths (Ratner and Castner, 2009). AR-XPS applied to phyllosilicates can provide information about ordering, layer thickness, and element and chemical state distributions within the layers (depth profile reconstruction). However, this technique requires a single crystal with a well ordered surface structure to generate a spectrum and that the possibility of signal observation from the mount is minimized (Ratner and Castner, 2009).

Detailed descriptions of XPS analytical strategies and sample preparation applied to the (001) surfaces of phyllosilicates are found in Biino and Groning (1998) and Elmi *et al.* (2013, 2014a, 2014b).

LITERATURE DATA

The chemical and physical properties of layer silicates indicate that bonding in the structure is highly anisotropic with bonding between sheets usually weaker than bonding between atoms within sheets. This anisotropy is responsible for the perfect cleavage and surface properties of phyllosilicates (Guggenheim, 2011).

Many solids exhibit a chemical composition at the surface that is different from that in the bulk as a result of, for example, oxidation, layering, and domain formation. In contrast, the surface composition of fresh-cleaved phyllosilicates has the overall composition of the bulk material (Stucki *et al.*, 1976; Elmi *et al.*, 2013, 2014a, 2014b), except for the surface oxygen concentrations, which tend to exceed the bulk value because of adsorbed species, such as atmospheric OH^- ions, CO_2, and/or water molecules. Christenson and Thomson (2016) observed that carbonate ions on air-cleaved mica surfaces result from reactions between atmospheric carbon dioxide and water catalyzed by the mica surface. The CO_2 would be expected to react at hydroxyl sites in the outermost tetrahedral sheet to form a bicarbonate species, which would then dissociate into a carbonate and a proton. These species would be stabilized near an aluminum site. The H^+ replaces the K^+ to maintain charge balance, and two K^+ with the carbonate then form K_2CO_3, which is mobile on or near the surface in the presence of water, but crystallizes under dry conditions (Christenson and Thomson, 2016). However, these authors did not consider the kinetics or the extent of carbonate ion formation.

Interlayer site: Potassium

Hydroxyl orientation has a major influence on ionic interlayer bonding strength in phyllosilicates because of the strong repulsion between hydrogen and the interlayer cation (Giese, 1977). For trioctahedral micas, in which the O-H vector of the OH group points directly into the interlayer site cavity, repulsion between hydroxyl groups and interlayer cations can play a significant role in the interlayer separation (Giese, 1975). Giese (1974) theoretically determined that the cleavage of dioctahedral and trioctahedral micas occurs along the plane containing the K^+ ions, which are equally distributed between both new surfaces. Elmi *et al.* (2014b) examined a complementary pair of cleaved polylithionite sample surfaces, which were in contact before splitting. The quantitative chemical compositions of both polylithionite surface pairs were approximately the same and indicate that about half of the interlayer cations remain on each surface in accordance with Giese (1974) as illustrated in Figure 1. Geatches and Wilcox (2014) created a variety of dioctahedral, interlayer (cation)-deficient 1*M* illite series models (*cis*-vacant, *trans*-vacant, single cell, sandwich, and mixed-layer relaxed models) via *ab initio* density functional theory (DFT). They observed that when the K−O distances and location are considered, the hydroxyl groups of the octahedral sheet determine the interlayer K^+ ion location for all model types. In the sandwich-relaxed models, relative to both the lower and upper layers, the K^+ ions lie directly above the hydroxyl group with the O-H vectors pointing downwards and upwards, respectively (Geatches and Wilcox, 2014).

From energy and symmetry considerations by LEED measurements on muscovite, Müller and Chang (1968) observed that the cleavage plane is a monolayer of K^+ ions, and that the cleavage K^+ ions are shared by the two cleavage faces. This monolayer of K^+ produces strong surface electric dipoles. Müller and Chang (1968) reported that the electric fields created during cleavage

https://doi.org/10.1346/CCMN.2016.064033 Published online by Cambridge University Press

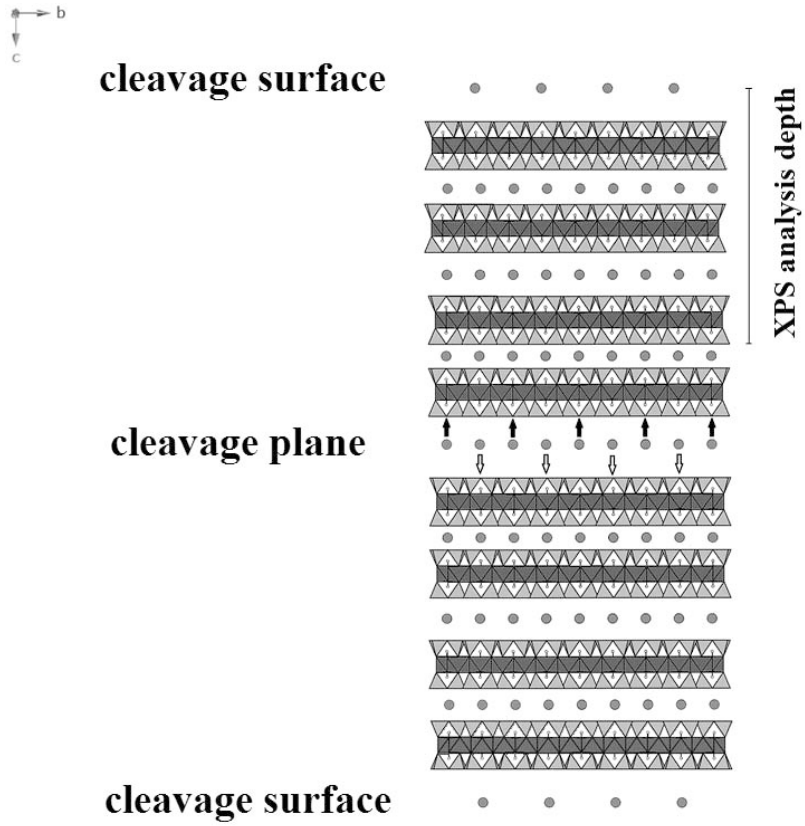

Figure 1. Model showing the XPS analysis depth in dioctahedral micas. Complementary pair of cleaved dioctahedral mica surfaces in contact before splitting. The K ions are shared equally between the separated surfaces, as determined by Giese (1974), Elmi *et al.* (2014b), Müller and Chang (1968), and Baun (1980). Conventional XPS analysis depth varies from 1 to 10 nm depending on material. For micas, the XPS analysis depth is about 1−5 nm. The apparent reduction of interlayer coordination number to eight observed by Elmi *et al.* (2013) and Elmi *et al.* (2014a) for muscovite and tetraferri-phlogopite (001) surfaces may be an average of the outermost interlayer surface and the next interlayer at about 10 Å depth.

affect these dipoles to varying degrees, depending on both the pressure and composition of the gases present during cleavage. The SIMS data collected by Baun (1980) for air-cleaved muscovite are consistent with the cleavage surface occupied by a K plane and the K^+ ions shared equally between the separated surfaces. The XPS binding energies for several phyllosilicates (Table 1) show that K exhibits a small chemical shift for the photoelectron line and the K_{2p} binding-energy values ranged from 293.0 to 294.5 eV. The highest values were

Table 1. Important K_{2p}-binding energies (in eV) for selected layer silicates.

Compound	$K_{2p_{3/2}}$ (eV)	Energy reference (eV)	References
Na-K-montmorillonite	293.1	Si_{2s} = 153.4	Seyama and Soma (1986)
K-montmorillonite	293.2	Si_{2s} = 153.4	Seyama and Soma (1986)
Biotite	293.3	C_{1s} = 284.6	Ilton and Veblen (1994)
Phlogopite	292.7	Si_{2s} = 153.4	Seyama and Soma (1986)
Phlogopite	293.0	C_{1s} = 284.6	Ilton and Veblen (1994)
Phengitic muscovite	293.26	Si_{2p} = 102.36	Biino and Groning (1998)
Sodian-muscovite	293.36	C_{1s} = 284.86	Elmi *et al.* (2013)
Tetraferri-phlogopite	293.6	C_{1s} = 284.8	Elmi *et al.* (2014a)
Fe-bearing phlogopite	294.5	C_{1s} = 284.8	Elmi *et al.* (2014a)
Polylithionite	293.3	C_{1s} = 285.1	Elmi *et al.* (2014b)
Fe^{2+}-rich polylithionite	293.3	C_{1s} = 285.1	Elmi *et al.* (2014b)

https://doi.org/10.1346/CCMN.2016.064033 Published online by Cambridge University Press

observed for tetraferri-phlogopite and Fe-bearing phlogopite, and these values may be related to the summed contributions from the tetrahedral and octahedral Fe^{3+} components.

LEED is widely used for directly characterizing the atomic structure of perfect surfaces. For silicates, Hochella *et al.* (1990) found that LEED can be performed at the low crossover voltage which is generally between 50 and 150 eV. However, this technique does not probe the local atomic structure, but considers an average structure sampled over a diameter of 1 mm and a depth of about 1 nm (Ash *et al.*, 1988). Moreover, the sample must be a single crystal with a well ordered surface structure to generate a back-scattered electron diffraction pattern. LEED techniques may also provide a quantitative crystallographic description of surface atomic positions.

The LEED diffraction patterns observed by Müller and Chang (1968, 1969), Dorel *et al.* (2000), and Ostendorf *et al.* (2008) on an air-cleaved muscovite surface revealed the usual hexagonal closest-packed periodicity based on Bragg reflections. Müller and Chang (1968, 1969) ascribed the triangular shape of Bragg spots in the muscovite surface LEED pattern to an effect caused by the deflection of electric fields parallel to the surface. These authors proposed that the electric fields arose from domains of oriented surface dipoles with features that were closely related to the surface structure. Dorel *et al.* (2000) observed that conventional LEED is usually not suitable for investigating defects located near the surface of micas because the bulk contribution masks layer contributions due to the finite penetration depth of low-energy electrons. These authors presented a novel experimental approach based upon a simple LEED device which modulated the electron-beam current to observe fine diffraction structures in an air-cleaved mica surface. Using this approach, Dorel *et al.* (2000) observed a series of rings at the topmost surface layers (*i.e.* "Henzler rings") of muscovite on a scale of 1–5 nm. Dorel *et al.* (2000) argued that these rings are defects resulting from the intrinsic arrangement of K at the terminal sheet, because the cleavage process is destructive and forms steps on the surface.

X-ray Photoelectron Diffraction (XPD) is another surface-sensitive technique and the term XPD is used for the diffraction effects observed in an XPS experiment. The XPD technique is more sensitive to chemically non-equivalent atomic species than XPS for the first few atomic layers. Because long-range order is not required, XPD is an atom-specific probe of short-range order to determine the local atomic arrangement of complicated materials, such as phyllosilicates (Ash *et al.*, 1988; Fadley, 1992; Evans and Hiorns, 1996).

Each type of atom has a unique diffraction signature associated with the surrounding neighbors (Fadley, 1992). Thus, XPD is a powerful tool to differentiate the octahedral cation sites in micas (Evans and Raftery, 1982; Ash *et al.*, 1987). Detailed XPD analytical strategies applied to phyllosilicate (001) surfaces are found in Evans *et al.* (1979), Evans and Raftery (1980), and Ash *et al.* (1988). For muscovite, Evans *et al.* (1979) observed that K^+ is twelve-fold coordinated in the outermost layers. This result is in contrast with the apparent reduction of interlayer-site coordination number to eight, which was observed by XPS for muscovite and tetraferri-phlogopite (001) surfaces by comparing binding energy values with literature data (Elmi *et al.*, 2013, 2014a). The XPS results may be an average of the outermost interlayer surface and the next interlayer at ~10 Å depth (Figure 1). The apparent coordination number reduction of the interlayer cation based on XPS is, however, consistent with a bond relaxation because the cleavage process is along the plane containing interlayer sites. The loss of interlayer cation–oxygen bonds may also produce tetrahedral sheet relaxation at the muscovite surface.

Tetrahedral sheet: Silicon and Aluminum

Silicon. The Si_{2p} binding energy of layer silicates, in which some Si is substituted by Al, is 0.7 eV lower than that of quartz or compounds containing only Si in the tetrahedral site (Table 2). The primary reason for the Si_{2p} binding energy decrease from quartz to phyllosilicates is the apparent reduction in the silica network polymerization driven by the Si content. The silicon binding energy shows that different populations of Si atoms correlate with substitutions in the layer and a lower Si_{2p} binding energy may result from a negative charge increase on the silicate framework by Si^{4+} replacement by $A1^{3+}$ and/or Fe^{3+}. This effect apparently occurs in saponite and in hectorite, where the negative charge is located in the tetrahedral SiO_4 sheet (substitution of Si^{4+} by Al^{3+}) and in the Mg octahedral sheet (substitution of Mg^{2+} by Li^+), respectively (Vantelon *et al.*, 2009). Seyama and Soma (1985) observed that the negative charge on the silicate framework is delocalized over Si, O, and tetrahedrally coordinated Al ions as a result of the systematic shifts of the photoelectron binding energies. Seyama and Soma (1985) observed that the Si_{2s} binding energy of phlogopite, in which isomorphic substitution of Si by Al occurs, is lower than that of a silicate in which isomorphic substitution does not occur. Seyama and Soma (1985) considered that this decrease of Si_{2s} binding energy results from an increase in the negative charge on the silicate framework because of the replacement of Si^{4+} by Al^{3+}. In contrast, Seyama and Soma (1985) deduced from photoelectron binding and Auger electron kinetic energies that the octahedrally coordinated Al and Mg ions in the silicate mineral are not subject to a strong effect from the negative charge on the silicate framework. Seyama and Soma (1985) found that the Al_{2p} binding energy of tetrahedrally coordinated Al ions decreases with decreasing Si_{2s} binding energy in montmorillonite, kaolinite, and phlogopite. This positive

https://doi.org/10.1346/CCMN.2016.064033 Published online by Cambridge University Press

Table 2. Important Si_{2p} binding energies (in eV) for selected layer silicates and quartz for Si in tetrahedral coordination.

Compound	Si_{2p} (eV)	Energy reference (eV)	References
SiO_2	103.5	C_{1s} = 284.6	Barr *et al.* (1995)
SiO_2	103.4	C_{1s} = 284.6	Briggs and Seah (1990); Barr *et al.* (1999)
SiO_2 α-cristobalite	103.25	C_{1s} = 284.6	Briggs and Seah (1990); Barr *et al.* (1999)
SiO_2 α-quartz	103.65	C_{1s} = 284.6	Briggs and Seah (1990); Barr *et al.* (1999)
Talc	103.13	C_{1s} = 284.6	Briggs and Seah (1990); Barr *et al.* (1999)
Phlogopite	102.1	C_{1s} = 284.6	Ilton and Veblen (1994)
Biotite	102.3	C_{1s} = 284.6	Ilton and Veblen (1994)
Sodian muscovite	102.1	C_{1s} = 284.86	Elmi *et al.* (2013)
Muscovite	102.36	C_{1s} = 284.8	Biino and Groning (1998)
Muscovite	102.65	C_{1s} = 284.4	Bhattacharyya (1993)
Margarite	102.36	C_{1s} = 284.8	Biino *et al.* (1999)
Kaolinite	102.7	C_{1s} = 284.4	Koppelman *et al.* (1980)
Kaolinite	102.75	C_{1s} = 284.6	Barr *et al.* (1995)
Montmorillonite	102.45	C_{1s} = 284.6	Barr *et al.* (1995)
Pyrophyllite	102.88	C_{1s} = 284.6	Briggs and Seah (1990); Barr *et al.* (1999)
Tetraferri-phlogopite	102.7	C_{1s} = 284.8	Elmi *et al.* (2014a)
Fe-bearing phlogopite	102.2	C_{1s} = 284.8	Elmi *et al.* (2014a)
Polylithionite	102.3	C_{1s} = 285.1	Elmi *et al.* (2014b)
Fe^{2+}-rich polylithionite	102.4	C_{1s} = 285.1	Elmi *et al.* (2014b)

correlation indicates that the Al_{2p} binding energy of the Al ion in tetrahedral sites of the phyllosilicates, as well as the Si_{2s} binding energy of the Si ion in tetrahedral sites, is influenced by the negative charge on the silicate framework (Seyama and Soma, 1985).

Using XPS, Elmi *et al.* (2014b) observed that a reduced and/or distorted coordination of tetrahedral cations at the surface of polylithionite-1*M* was produced after cleavage. This excess negative charge imbalance probably enhances the reactivity of the surface by attracting charged or polar (H_2O) molecules. This attraction may affect the coordination of tetrahedral cations at the crystal surface. Si_{2p}-XPS spectra show the main peak at a binding energy of 102.4 eV and a small peak at 99.4 eV for lepidolites (Elmi *et al.*, 2014b). A reduced Si cation coordination number at 99.4 eV suggests sputter damage to the air-cleaved surface by low energy Ar^+ ion bombardment.

Poppa and Elliot (1971) suggested the need to prevent beam damage to phyllosilicate surfaces particularly when these minerals are used in nucleation and growth process studies. These authors found that AES is a useful analytical tool to evaluate mica surfaces prior to and during the early stages of metal vapor deposition for epitaxial thin film growth. This technique focuses and scans the primary electron beam in the nanometer and micrometer range to analyze the top-most layers (2−10 atomic layers). The experimental setup is similar to that of a Scanning Electron Microscope (SEM), but in AES the electrons are used both for imaging and for chemical identification of the surface atoms. Auger transitions require a minimum of three electrons, thus, only elements with $Z \geqslant 3$ can be analyzed (Mathieu, 2009). With AES, Poppa and Elliot (1971) studied the surface composition of muscovite at the beginning of deposition by monitoring the substrate surface composition with AES analysis at several conditions (air-cleavage, Ultra-High Vacuum (UHV)-cleavage, muscovite surface heating at UHV or in oxygen). A limited number of Si^{4+} ions with reduced coordination (<4) were observed in muscovite. These authors observed using AES that near-surface Si was reduced from Si^{4+} to elemental Si and the uppermost K plane was depleted after extended exposure to a 1 keV electron beam with a current density of about 2×10^{-6} A/mm^2.

Aluminum. In layer silicates, Al atoms can occur in both tetrahedral and octahedral sites. A net negative charge in the tetrahedral sheet results from the replacement of tetrahedral Si^{4+} by Al^{3+} and/or Fe^{3+}, whereas a net negative charge in the octahedral sheet is generated by replacing the octahedral Al^{3+} ion by a divalent cation, such as Fe^{2+} or Mg^{2+}. The Al distribution affects surface charge distribution and magnitude, which influences phyllosilicate properties. For samples of phlogopite, vermiculite, and lithium-rich biotite, cleavage was found by XPD to occur in regions of high Al content (Evans *et al.*, 1979), whereas a lepidolite was shown to cleave preferentially in Mn-enriched regions (Evans and Raftery, 1982).

Several XPS studies attempted to distinguish the coordination environment of Al^{3+} in silicates (Table 3). Anderson and Swartz (1974) reported identical Al_{2p} binding energies for tetrahedral and octahedral aluminum in aluminosilicates. Ebina *et al.* (1997) and Barr *et al.* (1997) observed that the Al_{2p} binding energy increased with an increase in the ratio of octahedral to tetrahedral Al.

https://doi.org/10.1346/CCMN.2016.064033 Published online by Cambridge University Press

Table 3. Important Al_{2p} binding energies (in eV) for selected phases.

Compound	Al coordination	Al_{2p} (eV)	Energy reference (eV)	References
Al	metal	72.9	Au_{4f} = 84.0	Hinnen *et al.* (1994)
Al	metal	72.8	Au_{4f} = 84.0	Domen and Chuang (1989)
Al	metal	72.7	Au_{4f} = 84.0	Sarapatka (1993)
γ-Al_2O_3	octahedral	74.5	C_{1s} = 284.7	Strohmeier (1994)
γ-Al_2O_3	octahedral	73.9	C_{1s} = 284.4	Barr *et al.* (1997)
$Al(OH)_3$	octahedral	74.1	C_{1s} = 284.4	Barr *et al.* (1997)
Analcime	tetrahedral	73.9	C_{1s} = 284.4	Barr *et al.* (1997)
Sodalite	tetrahedral	73.6	C_{1s} = 284.4	Barr *et al.* (1997)
Saponite	tetrahedral	73.7	C_{1s} = 284.6	Ebina *et al.* (1997)
Kaolinite	octahedral	74.5	C_{1s} = 284.8	Remy *et al.* (1992)
Kaolinite	octahedral	74.7	C_{1s} = 284.8	Wagner *et al.* 1982
Kaolinite	octahedral	74.3	C_{1s} = 284.4	Barr *et al.* (1997)
Montmorillonite	octahedral	74.8	C_{1s} = 284.4	Barr *et al.* (1997)
Dioctahedral smectite	octahedral	74.5	C_{1s} = 284.6	Ebina *et al.* (1997)
Biotite	octahedral	74.0	C_{1s} = 284.6	Ilton and Veblen (1994)
Phengitic muscovite	octahedral	74.26	Si_{2p} = 102.36	Biino and Groning (1998)
Sodian-muscovite	octahedral	74.1	C_{1s} = 284.8	Elmi *et al.* (2013)
Phlogopite	tetrahedral and octahedral	73.8	C_{1s} = 284.6	Ilton and Veblen (1994)
Magnesium chlorite	tetrahedral and octahedral	74.1	C_{1s} = 284.6	Ebina *et al.* (1997)
Fe-bearing phlogopite	tetrahedral and octahedral	74.2	C_{1s} = 285.1	Elmi *et al.* (2014a)
Polylithionite	tetrahedral and octahedral	74.4	C_{1s} = 285.1	Elmi *et al.* (2014b)
Fe^{2+}-rich polylithionite	tetrahedral and octahedral	74.4	C_{1s} = 285.1	Elmi *et al.* (2014b)

Barr *et al.* (1997) noted that a more positive octahedral sheet character coupled with the relatively net negative tetrahedral sheet results in ionic Al–O bonds that are stronger in kaolinite and allophane than in Al_2O_3. This increase in Al_{2p} binding energy found for 1:1 layer minerals, such as kaolinite, should be enhanced for the 2:1 layer minerals, such as pyrophyllite or smectite. This enhancement is related to the octahedral sheet, which compensates for the charge of two adjacent negatively charged tetrahedral sheets. The greater ionic character of the Al–O bond is reflected in the higher Al_{2p} binding energy for montmorillonite (74.8 eV) in comparison to beidellitic montmorillonite (dioctahedral smectite with tetrahedral charge from Kunipia F; Kunimine Kogyo Co., Ebina *et al.*, 1997) and kaolinite (Barr *et al.*, 1997). Koppelman (1979) and Barr *et al.* (1997) suggested further that OH and/or F enhance the positive character of Al and result in a moderate increase in the Al_{2p} binding energy. The Al_{2p} spectra of Na-rich muscovite from Elmi *et al.* (2013) and Fe^{2+}-rich polylithionite from Elmi *et al.* (2014b) (Figure 2) show that the Al_{2p} binding energy increase results from an increase in silicate framework negative charge because of Si^{4+} replacement by Al^{3+}. Figure 3 shows that, in general, the Al_{2p} binding energy increased with increasing Al coordination. As the binding energies of Al_{2p} from the tetrahedral and octahedral Al atoms generally overlap, the deconvolution of the peak is problematic and makes distinguishing between four- and six-coordinated species difficult. Figure 3 shows that the binding energy values of Al_{2p} from both tetrahedral and octahedral Al atoms are intermediate between the octahedral and tetrahedral binding energy values. This effect is probably related to the overlap of Al_{2p} binding-energy values from the tetrahedral and octahedral Al atoms.

Biino and Groning (1998) and Elmi *et al.* (2013) showed that distinguishing between ^{IV}Al and ^{VI}Al contributions is not straightforward using a Gauss-Voigt deconvolution procedure. Barr *et al.* (1997) used an alternative identification approach based on the Al_{2p}/Si_{2p} full-width at half-maximum (FWHM). In aluminosilicates that contain only ^{VI}Al, the Al_{2p}/Si_{2p} FWHM ratio is approximately equal to one, whereas in aluminosilicates with both ^{IV}Al and ^{VI}Al, this ratio is apparently greater than one (Barr *et al.*, 1997). In muscovite, however, the Al_{2p}/Si_{2p} ratio is close to 1 (Al_{2p}/Si_{2p} = 1.02) and, therefore, this approach is not useful to distinguish the ^{IV}Al contribution from the greater ^{VI}Al contribution in phyllosilicates (Elmi *et al.*, 2013). Separation between the centers of the tetrahedral and octahedral Al contributions to the Al_{2p} peak must be sufficiently large relative to the Gaussian broadening to observe differences in Al contributions. A comprehensive Si/Al concentration profile as a function of depth should be developed in future studies to combine data from home laboratory XPS and synchrotron XPS. Bare *et al.* (2016) showed that, when the inelastic mean free path of the photoelectrons is considered, home laboratory aluminosilicate XPS does not provide a true measurement of the surface stoichiometry, whereas variable kinetic energy XPS provides a more surface sensitive

https://doi.org/10.1346/CCMN.2016.064033 Published online by Cambridge University Press

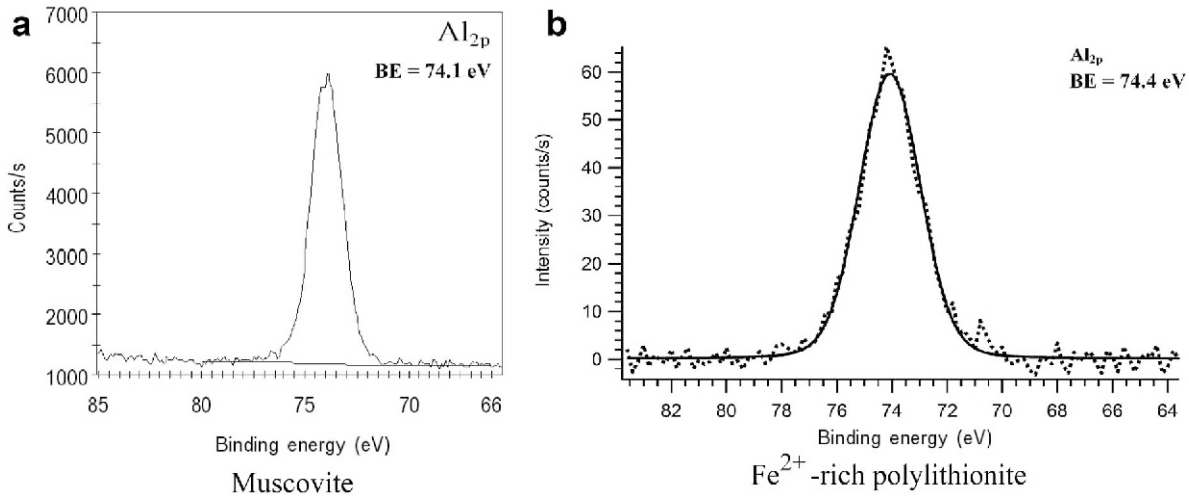

Figure 2. (a) Al_{2p} spectrum of Na-muscovite displayed as a plot of electron binding energy *vs.* intensity from Elmi *et al.* (2013). (b) Al_{2p} spectrum of Fe^{2+}-rich polylithionite displayed as a plot of electron binding energy *vs.* intensity from Elmi *et al.* (2014b). The Al_{2p} binding energy increase may result from an increase in the negative charge on the silicate framework because of Si^{4+} replacement by Al^{3+}.

measurement. The synchrotron data collected by Bare *et al.* (2016) were acquired at a water vapor partial pressure of 0.5 mbar and at a temperature of 225 ºC compared to the ultra-high vacuum and room temperature environment of the home laboratory XPS data, thereby making comparison difficult. For a true comparison of home laboratory XPS to synchrotron XPS studies, both data sets need to be collected under similar conditions.

The results reported by Ebina *et al.* (1997) show that DFT calculations are reliable tools to determine the qualitative distribution of octahedral and tetrahedral Al in phyllosilicates, and the technique produces a useful curve-fitting procedure. Evans and Raftery (1982) used XPD and observed that in lepidolite the octahedral Al sites are readily distinguished from the Li and Mn sites, and concluded that Al predominantly occupies *M*2 *cis* sites, whereas Li^{+} and Mn^{2+} prefer *M*1 *trans* sites. The XPD data collected by Evans and Raftery (1982) also showed that 40 ± 5% of the Al is tetrahedrally coordinated.

Octahedral sheet: Iron and Magnesium

Several studies used XPS to distinguish between Fe^{2+} and Fe^{3+} (Table 4). The Fe_{2p} spectra of silicate minerals

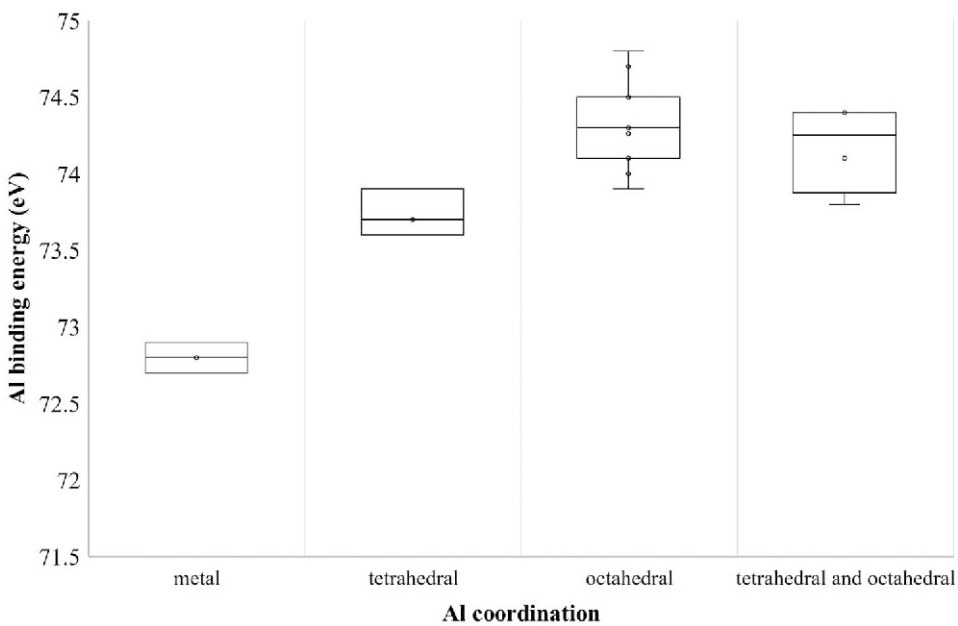

Figure 3. Relationship between Al coordination and Al_{2p}-binding energy on selected samples from the literature (data from Table 3).

https://doi.org/10.1346/CCMN.2016.064033 Published online by Cambridge University Press

Table 4. Important binding energies (in eV) for $Fe_{2p_{3/2}}$ peaks of selected Fe compounds.

Compound	Fe valence state	$Fe_{2p_{3/2}}$ (eV)	$Fe_{2p_{3/2}}$ satellite (eV)	Energy reference (eV)	References
Fe	0	706.70	–	C_{1s} = 284.60	Descostes *et al.* (2000)
Fe	0	706.8		C_{1s} = 285.0	Andersson and Howe (1989)
Fe	0	706.90	–	C_{1s} = 285.0	Brion (1980)
Fe	0	706.6		C_{1s} = 285.0	Langevoort *et al.* (1987)
Fe	0	706.5		C_{1s} = 285.0	Hawn and Dekoven (1987)
Fe	0	707.0		$Au_{4f_{7/2}}$ = 84.0	Mathieu and Landolt (1986)
Fe	0	707.5		$Au_{4f_{7/2}}$ = 84.0	Conner (1978)
Fe	0	706.8		$Au_{4f_{7/2}}$ = 84.0	Asami and Hashimoto (1977)
FeO	+II	709.85	715.50	C_{1s} = 284.60	Descostes *et al.* (2000)
FeO	+II	709.7		C_{1s} = 285.0	Hawn and Dekoven (1987)
FeO	+II	709.50	–	C_{1s} = 285.0	Brion (1980)
FeO (chromite)	+II	710.3		C_{1s} = 285.0	Langevoort *et al.* (1987)
FeF_2	+II	711.50	–	C_{1s} = 284.8	Grosvenor *et al.* (2004)
FeF_3	+III	715.10	724.0	C_{1s} = 284.8	Grosvenor *et al.* (2004)
FeF_3	+III	713.7			Hawn and Dekoven (1987)
$Fe_2(SO_4)_3$	+III	713.25	718.95	C_{1s} = 284.60	Descostes *et al.* (2000)
$Fe_2(SO_4)_3$	+III	713.5	–	C_{1s} = 285.0	Brion (1980)
Fe_2O_3	+III	711.4		C_{1s} = 285.0	Brion (1980)
Fe_2O_3	+III	711.2		C_{1s} = 285.0	Langevoort *et al.* (1987)
Fe_3O_4	+II	708.30	–	C_{1s} = 285.0	Brion (1980)
Fe_3O_4	+III	710.20	–	C_{1s} = 284.60	Descostes *et al.* (2000)
Fe_3O_4	+II	709.00	–	C_{1s} = 284.8	Grosvenor *et al.* (2004)
Fe_3O_4	+III	711.40	–	C_{1s} = 284.8	Grosvenor *et al.* (2004)
γ-FeOOH	+II	710.3	–	C_{1s} = 284.8	Grosvenor *et al.* (2004)
	+III	713.3	–	C_{1s} = 284.8	Grosvenor *et al.* (2004)
Iron sodium silicate glass	+II	709.7	715.0	C_{1s} = 284.6	Mekki *et al.* (1996)
	+III	711.2	719.0	C_{1s} = 284.6	Mekki *et al.* (1996)
Olivine $(Mg,Fe)_2SiO_4$	+II	710.4	–	$Au_{4f_{7/2}}$ = 84.0	Seyama and Soma (1987)
Nontronite	+III	711.8		$Au_{4f_{7/2}}$ = 83.9	Stucki *et al.* (1976)
Biotite	+II	708.6		$Au_{4f_{7/2}}$ = 83.9	Stucki *et al.* (1976)
	+III	711.0		$Au_{4f_{7/2}}$ = 83.9	Stucki *et al.* (1976)
Tetraferriphlogopite	+II	710.70	716.0	C_{1s} = 284.8	Elmi *et al.* (2014a)
	+III	712.5	720.0		Elmi *et al.* (2014a)
Fe-bearing phlogopite	+II	709.3	716.0	C_{1s} = 284.8	Elmi *et al.* (2014a)
	+III	712.5	720.0		Elmi *et al.* (2014a)
Polylithionite	+II	710.7	716.8	C_{1s} = 285.1	Elmi *et al.* (2014b)
	+III	713.0	730.0		Elmi *et al.* (2014b)
Fe^{2+}-rich polylithionite	+II	710.7	716.8	C_{1s} = 285.1	Elmi *et al.* (2014b)
	+III	713.0	730.0		Elmi *et al.* (2014b)

have satellite peaks that are characteristic of the different Fe oxidation states (Figure 4). Binding energies for Fe^{2+} are characteristically 2–3 eV lower than those for Fe^{3+}. According to several authors (Stucki et al., 1976; Biino and Groning, 1998; Grosvenor *et al.*, 2004; Elmi *et al.*, 2014a, 2014b), the peak at about 710 eV in unaltered trioctahedal micas is generally assigned to Fe^{3+}, and the small Fe^{2+} peak is generally assumed to be masked by the background of the larger Fe^{3+} peak (Figure 4). Table 4 compares the binding energies of $Fe_{2p_{3/2}}$ of select compounds containing Fe^{2+} and Fe^{3+}. In many cases, the dominating factor in the chemical shift is related to ion charge, whereby a more positive charge led to a more positive shift. The binding energy increased in the order Fe < Fe^{2+} < Fe^{3+} (Table 4), a trend that is clearly displayed in Figure 5 and that was also observed experimentally by Bancroft *et al.* (1979). One explanation of the observed shifts in Fe^{3+} and Fe^{2+} energies, where Fe is bonded to O, OH, or F, is related to changes in the coordination environment around the Fe ions as a result of oxidation and reduction reactions in biotite. Stucki *et al.* (1976) observed that the Fe^{3+} peak shift to lower binding energy indicates a change in coordination environment occurred upon oxidation. Stucki *et al.* (1976) observed that Fe^{3+} peaks occurred at 710.0 eV for unaltered biotite and at 709 eV for oxidized biotite. This result may be related to either Fe^{2+} in the structure or to a change in the Fe^{3+} coordination number as a result of the reduction reaction. Ash *et al.* (1988) observed that mirror plane characteristics of *C*2/*m* in the XPD data confirm that *M*2 and *M*3 are not differentiated in biotite.

https://doi.org/10.1346/CCMN.2016.064033 Published online by Cambridge University Press

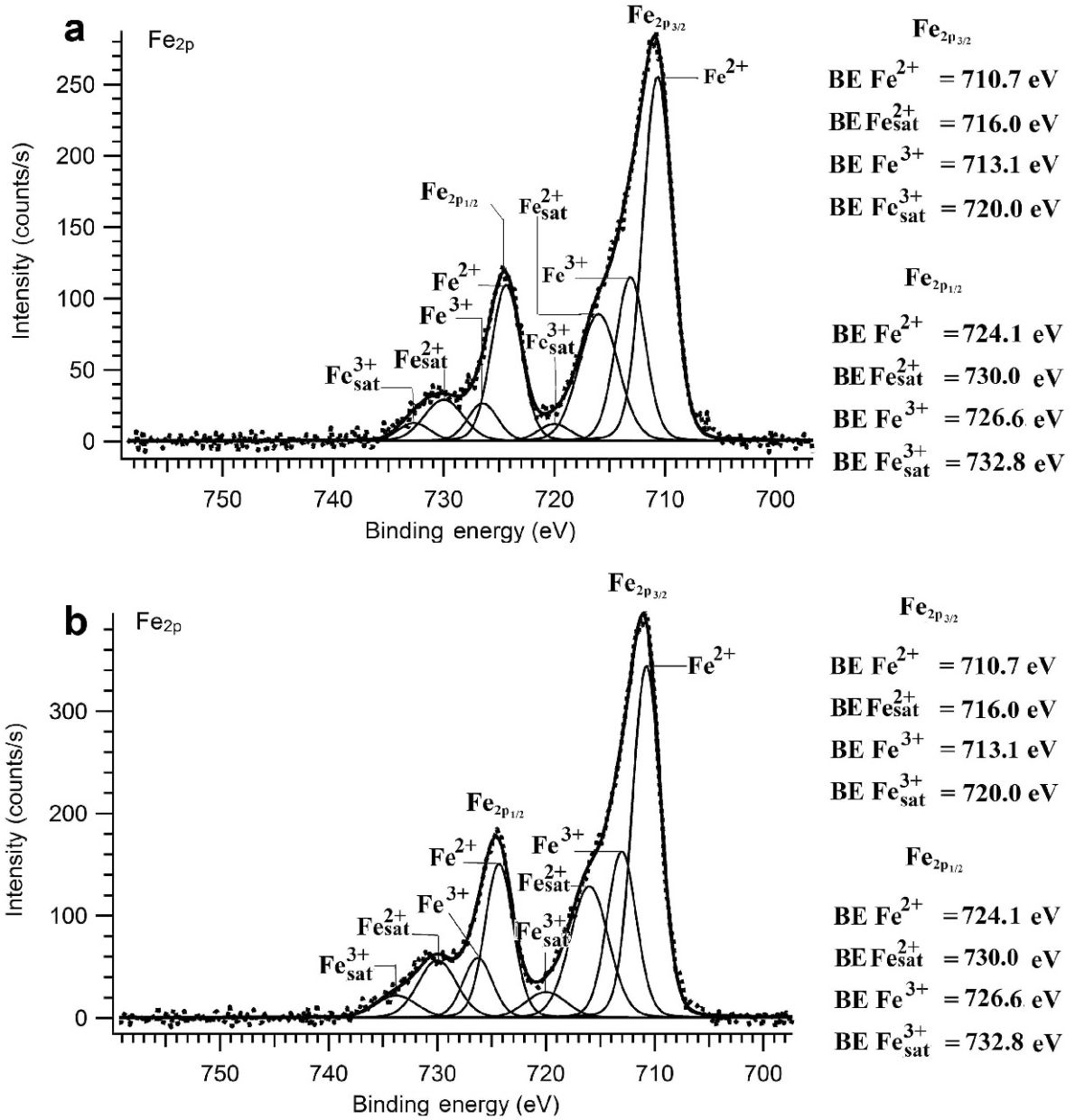

Figure 4. Fe_{2p} spectra (background subtracted) with the curve fit obtained for tetra-ferriphlogopite (a) and Fe bearing-phlogopite (b) from Elmi *et al.* (2014a). The deconvolution of the $Fe_{2p_{3/2}}$ peak (Binding Energy, BE = 712.5 eV) leads to two main components: one component is at BE = 710.7 eV with an associated satellite peak at BE = 716.0 eV, and the second component is at BE = 712.5 eV with an associated satellite peak at BE = 720.0 eV. Because of the inability to determine the contributions of each component following a Gauss-Voigt deconvolution procedure, the main $2p_{3/2}$ peak maximum at BE = 712.5 eV represents the summation of the tetrahedral and octahedral Fe^{3+} components.

The type and arrangement of the nearest-neighbor anions surrounding the cation and, in some cases, non-nearest neighbors, also influence the chemical shift (Haycock *et al.*, 1978; Seyama and Soma, 1984, 1985; Mittal *et al.*, 2004; Seyama *et al.*, 2006; Elmi *et al.*, 2014a). Koppelman (1979) observed that the electronegativity of anions (from O to F) further increase Mg and Al binding energies. Table 5 lists binding-energy values for select compounds studied by XPS, where Mg is bonded with OH or F anions. In brucite, $Mg(OH)_2$, (Haycock *et al.*, 1978) and Mg/Fe-rich spinel, $MgFe_2O_4$, (Mittal *et al.*, 2004), where Mg coordinates with OH groups or O, the binding energies are 1303.1 eV and 1302.7 eV, respectively. However, if O is substituted by F, the binding energy of Mg shifts to higher values (MgF_2, binding energy = 1306.5 eV, Seyama and Soma,

https://doi.org/10.1346/CCMN.2016.064033 Published online by Cambridge University Press

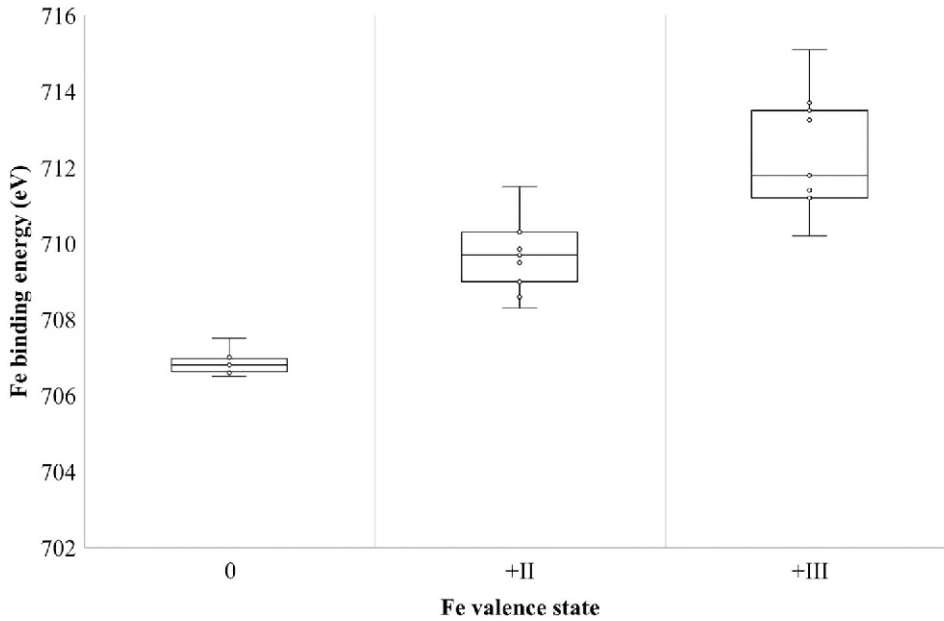

Figure 5. Relationship between Fe valence state and $Fe_{2p_{3/2}}$ binding energy on selected Fe compounds from the literature (data from Table 4).

1984). For tetra-ferriphlogopite and Fe-bearing phlogopite (1305.9 eV and 1306.8 eV, Elmi *et al.*, 2014a), Mg^{2+} ions in Fe-bearing phlogopite can be preferentially bonded to F over OH groups, in addition to O atoms.

CONCLUDING REMARKS

XPS data for fresh-cleaved phyllosilicates were described here to document that oxidation state, layer charge, and chemical bonding information can be obtained from the variations in binding energies ("chemical shifts") of different peaks. The type and arrangement of nearest-neighbor anions that surround the cation and, in some cases, non-nearest neighbors, also influence the chemical shift. Chemical shifts are sufficient to distinguish oxidation states and different chemical bonding to nearest neighbors. However, XPS cannot be used to distinguish different coordination environments of cations that are present both in tetrahedral and octahedral sites. The distribution of Al atoms affects the distribution and magnitude of the surface charge, which influences the properties of

Table 5. Important Mg_{2p} and Mg_{1s} binding energies (in eV) for selected layer silicates.

Compound	Mg coordination	Spectral line	Binding energy (eV)	Energy reference (eV)	References
Mg	metal	1s	1303.4	C_{1s} = 284.00	Steiner *et al.* (1978)
Mg	metal	2p	49.30	C_{1s} = 284.00	Jerome *et al.* (1986)
MgO	octahedral	1s	1303.9	Au_{4f} = 84.00	Seyama & Soma, 1984
MgO	octahedral	2p	50.25	C_{1s} = 284.00	Jerome *et al.* (1986)
$Mg(OH)_2$	octahedral	1s	1302.7	C_{1s} = 284.50	Haycock *et al.* (1978)
$Mg(OH)_2$	octahedral	2p	49.50	C_{1s} = 284.50	Haycock *et al.* (1978)
MgF_2	octahedral	1s	1304.95	C_{1s} = 284.45	Wagner (1980)
MgF_2	octahedral	2p	51.95	C_{1s} = 284.45	Wagner (1980)
Talc	octahedral	2p	50.46	C_{1s} = 284.60	Wagner *et al.* (1982)
Montmorillonite	octahedral	1s	1305.3	Au_{4f} = 84.00	Seyama and Soma (1984)
Phlogopite	octahedral	1s	1303.7	Au_{4f} = 84.00	Seyama and Soma (1985)
Phengitic muscovite	octahedral	2p	50.55	Si_{2p} = 102.36	Biino and Groning (1998)
Biotite	octahedral	2p	50.20	C_{1s} = 284.6	Ilton and Veblen (1994)
Phlogopite	octahedral	2p	49.60	C_{1s} = 284.6	Ilton and Veblen (1994)
Tetraferriphlogopite	octahedral	1s	1305.9	C_{1s} = 284.8	Elmi *et al.* (2013)
Fe-bearing phlogopite	octahedral	1s	1306.8	C_{1s} = 284.8	Elmi *et al.* (2013)

https://doi.org/10.1346/CCMN.2016.064033 Published online by Cambridge University Press

phyllosilicates. Although several XPS studies attempted to distinguish the coordination environment of Mg^{2+} and Al^{3+} in silicates, the binding-energy values of Al_{2p} indicate that when ^{IV}Al and ^{VI}Al occur together, the sites cannot be clearly distinguished. With respect to XPS, XPD has the great advantage over XPS of being sensitive to local short-range atomic arrangements in phyllosilicates. X-ray photoelectron diffraction, thus, is useful to discriminate between different Al coordination numbers as detected in biotite.

Several authors observed that the negative layer charge on the silicate framework is delocalized over Si, O, and ^{IV}Al ions owing to the systematic shifts of photoelectron binding energies. The chemical shift of the Si_{2p} binding energy to lower binding-energy values may result from an increase in the negative layer charge in the silicate framework because of Si^{4+} replacement by Al^{3+} and/or Fe^{3+}. The Al_{2p} binding energy of tetrahedrally coordinated Al ions in montmorillonite, kaolinite, and phlogopite decreases with decreases in Si_{2s} binding energy. This positive correlation indicates that the silicate framework negative charge influences the Al_{2p} and Si_{2s} binding energies of Al and Si ions in tetrahedral sites.

The attraction of polar H_2O molecules after cleavage produces a reduced and/or distorted coordination of tetrahedral cations at the crystal surface. Several authors reported that the binding energy of Mg depends on the chemistry of the anion site and the local environment around the cation site. If O is substituted by F, the binding energy of Mg is shifted to higher values.

This paper presents different viewpoints on the cleavage mechanism obtained from different surface-sensitive techniques. LEED and SIMS measurements on air-cleaved muscovite surfaces have shown that cleavage occurs along the K plane and the K^+ ions were shared equally between the separated surfaces. Quantitative XPS analyses for polylithionite surface pairs are approximately identical, indicating that about half of the interlayer cations remain on each surface, which is consistent with LEED and SIMS data and with theoretical models.

XPD experiments on muscovite suggest that K^+ is twelve-fold coordinated nearest to the outermost layers. The apparent reduction of interlayer coordination number to eight at the surface, which was observed by XPS for muscovite and tetraferri-phlogopite (001) surfaces, is consistent with bond relaxation due to cleavage along the plane that contains interlayer sites. The loss of interlayer cation–oxygen bonds may also produce a tetrahedral sheet relaxation at the muscovite surface.

This review highlights progress that has been achieved in the last decades to clarify structural aspects of freshly cleaved phyllosilicate surfaces by the use of surface-sensitive techniques. Surface crystal chemical studies of phyllosilicates that are cleaved in air promise to significantly advance both pure and applied science, and these studies will have a substantial impact on future technology. Much remains to be studied to fully understand cleavage mechanisms, surface layer charge, different cation coordination environments in both tetrahedral and octahedral sites, and the possible presence of interlayer domains. Conventional XPS, which is characterized by a fixed photon energy, limited energy resolution, and larger spot size may discriminate between different atoms and the surface oxidation state, but a large crystal size is required. Reducing electron spot size will reduce the count rate and limit the quality of the investigation. The possibility to tune photon energy to increase the photoionization cross-section, to enhance energy resolution, and to reduce spot size is available at third generation synchrotron radiation facilities. Thus, synchrotron use could distinguish between the coordination environments of Mg^{2+} and Al^{3+} in silicates. A comprehensive elemental concentration profile as a function of depth may be developed combining the data from home laboratory XPS and synchrotron XPS in future experiments. Moreover, the possibility to tune the XPS surface sensitivity/sampling-depth by varying the acquisition conditions (*i.e.*, fluorescence, total/partial electron yield, grazing incidence conditions) may improve the knowledge of phyllosilicate surface properties. The potential roles of irregular surface topologies on coordination environments and bonding should also be explored in future experiments.

ACKNOWLEDGMENTS

The authors are grateful to three anonymous reviewers as well as the Editor-in-Chief, Joseph W. Stucki and the Associate Editor, Ravi Kukkadapu, for the critical reading of the manuscript and their thoughtful and constructive reviews.

REFERENCES

Anderson, P.R. and Swartz, W.E. (1974) X-ray photoelectron spectroscopy of some aluminosilicates. *Inorganic Chemistry*, **13**, 2293–2294.

Andersson, S.L.T. and Howe, R.F. (1989) An X-ray photoelectron study of metal clusters in zeolites. *The Journal of Physical Chemistry*, **93**, 4913–4920.

Asami, K. and Hashimoto, K. (1977) The X-ray photoelectron spectra of several oxides of iron and chromium. *Corrosion Science*, **17**, 559–570.

Ash, L.A., Evans, S., and Hiorns, A.G. (1987) Cation ordering in lepidolite and biotite studied by XPD. *Clay Minerals*, **22**, 375–386.

Ash, L.A., Clark, S.L., Evans, S., and Hiorns, A.G. (1988) X-ray photoelectron diffraction studies of the micas lepidolite and biotite. *Journal of the Chemical Society-Dalton Transactions*, **4**, 859–879.

Bancroft, G.M., Brown, J.R., and Fyfe, W.S. (1979) Advances in and applications of X-ray photoelectron spectroscopy (ESCA) in mineralogy and geochemistry. *Chemical Geology*, **25**, 227–243.

Bare, S. R., Knop-Gericke, A., Teschner, D., Havacker, M., Blume, R., Rocha, T., Schloegl, R., Chan, A. S. Y., Blackwell, N., Charochak, M. E., ter Veen, R., and

Brongersma, H. H. (2016) Surface analysis of zeolites: An XPS, variable kinetic energy XPS, and low energy ion scattering study. *Surface Science*, **648**, 376–382.

Barr, T.L., Seal, S., He, H., and Klinowski, J. (1995) X-ray photoelectron spectroscopic studies of kaolinite and montmorillonite. *Vacuum*, **46**, 1391–1395.

Barr, T.L., Seal, S., Wozniak, K., and Klinowski, J. (1997) ESCA studies of the coordination state of aluminium in oxide environments. *Journal of the Chemical Society, Faraday Transactions*, **93**, 181–186.

Barr, T.L., Hoppe, E., Dugall, T., Shah, P., and Seal, S. (1999) XPS and bonding: When and why can relaxation effects be ignored. *Journal of Electron Spectroscopy and Related Phenomena*, **98–99**, 95–103.

Baun, W.L. (1980) ISS/SIMS characterization of mica surfaces. *Surface and Interface Analysis*, **2**, 145–147.

Beaulieu, B.T. and Savage, K.S. (2005) Arsenate adsorption structures on aluminum oxide and phyllosilicate mineral surfaces in smelter-impacted soils. *Environmental Science & Technology*, **39**, 3571–3579.

Bhattacharyya, K.G. (1993) XPS study of mica surfaces. *Journal of Electron Spectroscopy and Related Phenomena*, **63**, 289–306.

Biino, G.G. and Groning, P. (1998) Cleavage mechanism and surface chemical characterization of phengitic muscovite and muscovite as constrained by X-ray photoelectron spectroscopy. *Physics and Chemistry of Minerals*, **25**, 168–181.

Biino, G.G., Mannella, N., Kay, A., Mun, B., and Fadley, C.S. (1999) Surface chemical characterization and surface diffraction effects of real margarite (001): An angle-resolved XPS investigation. *American Mineralogist*, **84**, 629–638.

Brigatti, M.F., and Guggenheim, S. (2002) Mica crystal chemistry and the influence of pressure, temperature, and solid solution on atomistic models. In Micas: crystal chemistry and metamorphic petrology. Pp. 1–97 in: *Micas: Crystal Chemistry and Metamorphic Petrology* (A. Mottana, F.P. Sassi, J.B. Thompson Jr., and S. Guggenheim, editors). Reviews in Mineralogy and Geochemistry, **46**. Mineralogical Society of America and the Geochemical Society, Washington, D.C.

Brigatti, M.F., Malferrari, D., Laurora, A., and Elmi, C. (2011) Structure and mineralogy of layer silicates: recent perspectives and new trends. Pp. 1–71 in: *Layered Mineral Structures and their Application in Advanced Technologies* (M.F. Brigatti and A. Mottana, editors). EMU Notes in Mineralogy, **11**. The Mineralogical Society of Great Britain & Ireland.

Briggs, D. and Seah, M.P. (1990) *Practical Surface Analysis, second edition, Vol. 1. Auger and X-ray Photoelectron Spectroscopy*. John Wiley & Sons, Chichester, UK.

Brion, D. (1980) Etude par spectroscopie de photoelectrons de la degradation superficielle de FeS'' CuFeS'', ZnS, and PbS a l'air dans l'eau. *Applied Surface Science*, **5**, 133–152.

Bronold, M., Tomm, Y., and Jaegermann, W. (1994) Surface states on cubic d-band semiconductor pyrite (FeS_2). *Surface Science*, **314**, L931–L936.

Carretero, M.I. and Pozo, M. (2009) Clay and non-clay minerals in the pharmaceutical industry part I. Excipients and medical applications. *Applied Clay Science*, **46**, 73–80.

Carretero, M.I. and Pozo, M. (2010) Clay and non-clay minerals in the pharmaceutical and cosmetic industries part II. Active ingredients. *Applied Clay Science*, **47**, 171–181.

Chan, D. and Richmond, P. (1977) Van der Waals forces for mica and quartz: Calculations from complete dielectric data. *Proceedings of the Royal Society of London A: Mathematical, Physical and Engineering Sciences*, **353**, 163–176.

Christenson, H.K. (1993) Adhesion and surface energy of mica in air and water. *The Journal of Physical Chemistry*, **97**, 12034–12041.

Christenson, H.K., and Thomson, N.H. (2016) The nature of the air-cleaved mica surface. *Surface Science Reports*, **71**, 367–390.

Conner, G.R. (1978) Combination analysis of metal oxides using ESCA, AES, and SIMS. *Journal of Vacuum Science and Technology*, **15**, 343–347.

Czímerová, A., Bujdák, J., and Dohrmann, R. (2006) Traditional and novel methods for estimating the layer charge of smectites. *Applied Clay Science*, **34**, 2–13.

Descostes, M., Mercier, F., Thromat, N., Beaucaire, C., and Gautier-Soyer, M. (2000) Use of XPS in the determination of chemical environment and oxidation state of iron and sulfur samples: Constitution of a data basis in binding energies for Fe and S reference compounds and applications to the evidence of surface species of an oxidized pyrite in a carbonate medium. *Applied Surface Science*, **165**, 288–302.

Domen, K. and Chuang, T.J. (1989) Laser induced photodissociation and desorption. II. CH_2I_2 adsorbed on Ag. *The Journal of Chemical Physics*, **90**, 3332–3338.

Dorel, S., Pesty, F., and Garoche, P. (2000) Oscillating low-energy electron diffraction for studying nanostructured surfaces. *Surface Science*, **446**, 294–300.

Ebina, T., Iwasaki, T., Chatterjee, A., Katagiri, M., and Stucky, G.D. (1997) Comparative study of XPS and DFT with reference to the distributions of Al in tetrahedral and octahedral sheets of phyllosilicates. *Journal of Physical Chemistry B*, **101**, 1125–1129.

Elmi, C., Brigatti, M.F., Guggenheim, S., Pasquali, L., Montecchi, M., Laurora, A., Malferrari, D., and Nannarone, S. (2013) Sodian muscovite-$2M_1$: Crystal chemistry and surface features. *The Canadian Mineralogist*, **51**, 319–328.

Elmi, C., Brigatti, M.F., Guggenheim, S., Pasquali, L., Montecchi, M., and Nannarone, S. (2014a) Crystal chemistry and surface configurations of two iron-bearing trioctahedral mica-1M polytypes. *Clays and Clay Minerals*, **62**, 243–252.

Elmi, C., Brigatti, M.F., Guggenheim, S., Pasquali, L., Montecchi, M., and Nannarone, S. (2014b) Crystal chemistry and surface configurations of two polylithionite-1M crystals. *American Mineralogist*, **99**, 2049–2059.

Evans, S. and Hiorns, A.G. (1996) Angle-resolved X-ray photoelectron studies of cleavage in chlorites. *Clays and Clay Minerals*, **44**, 398–407.

Evans, S. and Raftery, E. (1980) X-ray photoelectron studies of titanium in biotite and phlogopite. *Clay Minerals*, **15**, 209–218.

Evans, S. and Raftery, E. (1982) X-ray photelectron diffraction studies of lepidolite. *Clay Minerals*, **17**, 443–452.

Evans, S., Adams, J.M., and Thomas, J.M. (1979) The surface structure and composition of layered silicate minerals: Novel insights from X-ray photoelectron diffraction, K-emission spectroscopy and cognate techniques. *Philosophical Transactions of the Royal Society A: Mathematical, Physical and Engineering Sciences*, **292**, 563–591.

Fadley, C.S. (1992) The study of surface structures by photoelectron diffraction and Auger electron diffraction. Pp. 421–518 in: *Synchrotron radiation research: Advances in surface and interface science techniques* (R.Z. Bachrach, editor) Springer US, Boston, MA, USA..

Fenter, P. and Sturchio, N.C. (2004) Mineral–water interfacial structures revealed by synchrotron X-ray scattering. *Progress in Surface Science*, **77**, 171–258.

Fu, Y.-T., Zartman, G.D., Yoonessi, M., Drummy, L.F., and Heinz, H. (2011) Bending of layered silicates on the

https://doi.org/10.1346/CCMN.2016.064033 Published online by Cambridge University Press

nanometer scale: Mechanism, stored energy, and curvature limits. *The Journal of Physical Chemistry C*, **115**, 22292–22300.

Geatches, D.L. and Wilcox, J. (2014) *Ab initio* investigations of dioctahedral interlayer-deficient mica: Modelling 1*M* polymorphs of illite found within gas shale. *European Journal of Mineralogy*, **26**, 127–144.

Gershenkop, A.S., Gerasimova, L.G., Khokhulya, M.S., Zhdanova, N.M., and Okhrimenko, R.F. (2001) Preparation of flaky pearly pigments. *Inorganic Materials*, **37**, 531–534.

Giese, R.F., Jr. (1974) Surface energy calculations for muscovite. *Nature*, **248**, 580–581.

Giese, R.F., Jr. (1975) The effect of F/OH substitution on some layer-silicate minerals. *Zeitschrift für Kristallographie - Crystalline Materials*, **141**, 138–144.

Giese, R.F., Jr. (1977) The influence of hydroxyl orientation, stacking sequence, and ionic substitutions on the interlayer bonding of micas. *Clays and Clay Minerals*, **25**, 102–104.

Giese, R.F., Jr. (1978) The electrostatic interlayer forces of layer structure minerals. *Clays and Clay Minerals*, **26**, 51–57.

Grosvenor, A.P., Kobe, B.A., Biesinger, M.C., and McIntyre, N.S. (2004) Investigation of multiplet splitting of Fe_{2p} XPS spectra and bonding in iron compounds. *Surface and Interface Analysis*, **36**, 1564–1574.

Guggenheim, S. (2011) An overview of order/disorder in hydrous phyllosilicates. Pp. 72-111 in: *Layered Mineral Structures and their Application in Advanced Technologies* (M.F. Brigatti and A. Mottana, editors). EMU Notes in Mineralogy, **11**, European Mineralogical Union and the Mineralogical Society of Great Britain & Ireland.

Gutshall, P.L., Bryant, P.J., and Cole, G.M. (1970) Cleavage surface energy of phlogopite mica. *American Mineralogist*, **55**, 1432–1434.

Hawn, D.D. and Dekoven, B.M. (1987) Deconvolution as a correction for photoelectron inelastic energy-losses in the core level XPS spectra of iron-oxides. *Surface and Interface Analysis*, **10**, 63–74.

Haycock, D.E., Kasrai, M., Nicholls, C.J., and Urch, D.S. (1978) The electronic structure of magnesium hydroxide (brucite) using X-ray emission, X-ray photoelectron, and Auger spectroscopy. *Journal of the Chemical Society, Dalton Transactions*, **12**, 1791–1796.

Hinnen, C., Imbert, D., Siffre, J.M., and Marcus, P. (1994) An in situ XPS study of sputter-deposited aluminium thin films on graphite. *Applied Surface Science*, **78**, 219–231.

Hochella, M.F. (1990) Atomic structure, microtopography, composition, and reactivity of mineral surfaces. Pp. 87–132 in: *Mineral-water interface geochemistry* (M.F.J. Hochella, and A.F. White, editors), Reviews in Mineralogy and Geochemistry, **23**, Mineralogical Society of America and the Geochemical Society, Washington, D.C.

Hochella, M.F.J. (1995) Mineral surfaces: Their characterization and their chemical, physical and reactive nature. pp. 17–60 in: *Mineral Surfaces* (D.J. Vaughan, and R.A.D. Pattrick, editors). The Mineralogical Society Series, **5**. The Mineralogical Society of Great Britain & Ireland. London.

Ilton, E.S. and Veblen, D.R. (1994) Chromium sorption by phlogopite and biotite in acidic solutions at 25ºC: Insights from X-ray photoelectron spectroscopy and electron microscopy. *Geochimica et Cosmochimica Acta*, **58**, 2777–2788.

Ilton, E.S., Moses, C.O., and Veblen, D.R. (2000) Using X-ray photoelectron spectroscopy to discriminate among different sorption sites of micas: With implications for heterogeneous reduction of chromate at the mica-fluid interface. *Geochimica et Cosmochimica Acta*, **64**, 1437–1450.

Jerome, R., Teyssie, P., Pireaux, J.J., and Verbist, J.J. (1986) Surface-analysis of polymers end-capped with metal carboxylates using X-ray photoelectron spectroscopy. *Applied Surface Science*, **27**, 93–105.

Junru, T., Yunfang, H., Wenxiang, H., Xiuzeng, C., and Xiansong, F. (2002) The preparation and characteristics of cobalt blue mica coated titania pearlescent pigment. *Dyes and Pigments*, **52**, 215–222.

Kerkhof, F.P.J.M. and Moulijn, J.A. (1979) Quantitative analysis of xps intensities for supported catalysts. *The Journal of Physical Chemistry*, **83**, 1612–1619.

Koppelman, M.H. (1979) Application of X-ray photoelectron spectroscopy to the study of mineral surface chemistry. pp. 205–242 in: *Advanced Chemical Methods for Soil and Clay Mineral Research: Proceedings of the NATO Advanced Study Institute held at the University of Illinois, July 23 - August 4, 1979* (J.W. Stucki and W.L. Banwart, editors). D. Reidel Publishing Company.

Koppelman, M.H., Emerson, A.B., and Dillard, J.G. (1980) Adsorbed Cr(III) on chlorite, illite, and kaolinite. *Clays and Clay Minerals*, **28**, 119–124.

Kuwahara, Y. (1999) Muscovite surface structure imaged by fluid contact mode AFM. *Physics and Chemistry of Minerals*, **26**, 198–205.

Kuwahara, Y. (2001) Comparison of the surface structure of the tetrahedral sheets of muscovite and phlogopite by AFM. *Physics and Chemistry of Minerals*, **28**, 1–8.

Langevoort, J.C., Sutherland, I., Hanekamp, L.J., and Gellings, P.J. (1987) On the oxide formation on stainless steels AISI 304 and incoloy 800H investigated with XPS. *Applied Surface Science*, **28**, 167–179.

Lee, S.S., Fenter, P., Park, C., Sturchio, N.C., and Nagy, K.L. (2010) Hydrated cation speciation at the muscovite (001)-water interface. *Langmuir*, **26**, 16647–16651.

Lee, S.S., Fenter, P., Nagy, K.L. and Sturchio, N.C. (2012) Monovalent ion Adsorption at the muscovite (001–solution interface: Relationships among ion coverage and speciation, interfacial water structure, and substrate relaxation. *Langmuir*, **28**, 8637–8650.

Lee, S.S., Schmidt, M., Laanait, N., Sturchio, N.C., and Fenter, P. (2013) Investigation of structure, adsorption free energy, and overcharging behavior of trivalent yttrium adsorbed at the muscovite (001)–water interface. *The Journal of Physical Chemistry C*, **117**, 23738–23749.

Maisch, R., Stahlecker, O., and Kieser, M. (1996) Mica pigments in solvent free coatings systems. *Progress in Organic Coatings*, **27**, 145–152.

Marcelli, A., Cibin, G., Cinque, G., Mottana, A., and Brigatti, M. F. (2006) Polarized XANES spectroscopy: The K edge of layered K-rich silicates. *Radiation Physics and Chemistry*, **75**, 1596–1607.

Mathieu, H.J. (2009) Auger electron spectroscopy. Pp. 9–45 in: *Surface Analysis – The Principal Techniques, 2nd Edition*. (J.C. Vickerman and I.S. Gilmore, Editors), John Wiley & Sons, Ltd.

Mathieu, H.J. and Landolt, D. (1986) An investigation of thin oxide films thermally grown *in situ* on Fe-24Cr and Fe-24Cr-11Mo by Auger electron spectroscopy and X-ray photoelectron spectroscopy. *Corrosion Science*, **26**, 547–559.

Maurice, P.A. (2009) *Environmental Surfaces and Interfaces. From the Nanoscale to the Global Scale.* John Wiley & Sons, Ltd.

Mekki, A., Holland, D., McConville, C.F., and Salim, M. (1996) An XPS study of iron sodium silicate glass surfaces. *Journal of Non-Crystalline Solids*, **208**, 267–276.

Metsik, M.S. (1972) Splitting of mica crystals and surface energy. *The Journal of Adhesion*, **3**, 307–314.

Mittal, V.K., Bera, S., Nithya, R., Srinivasan, M.P., Velmurugan, S., and Narasimhan, S.V. (2004) Solid state synthesis of Mg-Ni ferrite and characterization by XRD and XPS. *Journal of Nuclear Materials*, **335**, 302–310.

Moore, D.E. and Lockner, D.A. (2004) Crystallographic controls on the frictional behavior of dry and water-saturated sheet structure minerals. *Journal of Geophysical Research*, **109**, B03401.

Müller, K. and Chang, C.C. (1968) Low energy electron diffraction observations of electric dipoles on mica surfaces. *Surface Science*, **8**, 455–458.

Müller, K. and Chang, C.C. (1969) Electric dipoles on clean mica surfaces. *Surface Science*, **14**, 39–51.

Obreimoff, J.W. (1930) The splitting strength of mica. *Proceedings of the Royal Society of London A: Mathematical, Physical and Engineering Sciences*, **127**, 290–297.

Ostendorf, F., Schmitz, C., Hirth, S., Kuhnle, A., Kolodziej, J.J., and Reichling, M. (2008) How flat is an air-cleaved mica surface? *Nanotechnology*, **19**, 305705.

Poppa, H. and Elliot, A.G. (1971) The surface composition of mica substrates. *Surface Science*, **24**, 149–163.

Ratner, B.D. and Castner, D.G. (2009) Electron spectroscopy for chemical analysis. pp. 47–112 in: *Surface Analysis – The Principal Techniques, 2nd Edition*. (J.C. Vickerman and I.S. Gilmore, Editors), John Wiley & Sons, Ltd..

Remy, M.J., Genet, M.J., Poncelet, G., Lardinois, P.F., and Notte, P.P. (1992) Investigation of dealuminated mordenites by X-ray photoelectron spectroscopy. *The Journal of Physical Chemistry*, **96**, 2614–2617.

Sakuma, H. (2013) Adhesion energy between mica surfaces: Implications for the frictional coefficient under dry and wet conditions. *Journal of Geophysical Research: Solid Earth*, **118**, 6066–6075.

Sarapatka, T.J. (1993) Palladium-induced charge transports with palladium/alumina/aluminum interface formation. *The Journal of Physical Chemistry*, **97**, 11274–11277.

Seyama, H. and Soma, M. (1984) X-ray photoelectron spectroscopic study of montmorillonite containing exchangeable divalent cations. *Journal of the Chemical Society, Faraday Transactions 1: Physical Chemistry in Condensed Phases*, **80**, 237–248.

Seyama, H. and Soma, M. (1985) Bonding-state characterization of the constitutent elements of silicate minerals by X-ray photoelectron spectroscopy. *Journal of Chemical Society, Faraday Transactions I*, **81**, 485–495.

Seyama, H. and Soma, M. (1986) X-ray photoelectron spectroscopic study of the effect of heating on montmorillonite containing sodium and potassium cations. *Clays and Clay Minerals*, **34**, 672–676.

Seyama, H. and Soma, M. (1987) Fe_{2p} spectra of silicate minerals. *Journal of Electron Spectroscopy and Related Phenomena*, **42**, 97–101.

Seyama, H. and Soma, M. (2003) Surface-analytical studies on environmental and geochemical surface processes. *Analytical Sciences*, **19**, 487–497.

Seyama, H., Soma, M., and Theng, B.K.G. (2006) X-ray photoelectron spectroscopy. Pp. 865–878. In *Handbook of Clay Science* (F. Bergaya, B.K.G. Theng, and G. Lagaly, editors). Developments in Clay Science, **1**, Elsevier.

Shaw, S.A., Peak, D., Hendry, M.J. (2009) Investigation of acidic dissolution of mixed clays between pH 1.0 and −3.0 using Si and Al X-ray absorption near edge structure. *Geochimica et Cosmochimica Acta*, **73**, 4151–4165

Somorjai, G.A. and Li, Y. (2011) Impact of surface chemistry. *Proceeding of the National Academy of Science of the United States of America*, **108**, 917–924.

Steiner, P., Reiter, F.J., Höchst, H., Hüfner, S., and Fuggle, J.C. (1978) Lineshape of the KL2L3(1D2) auger line in magnesium and sodium metal. *Physics Letters A*, **66**, 229–232.

Strohmeier, B.R. (1994) Characterization of an activated alumina claus catalyst by XPS. *Surface Science Spectra*, **3**, 141–146.

Stucki, J.W., Roth, C.B., and Baitinger, W.E. (1976) Analysis of iron-bearing clay minerals by ESCA. *Clays and Clay Minerals*, **24**, 289–292.

Tenório Cavalcante, P.M., Dondi, M., Guarini, G., Barros, F.M., and Benvindo da Luz, A. (2007) Ceramic application of mica titania pearlescent pigments. *Dyes and Pigments*, **74**, 1–8.

Vantelon, D., Belkhou, R., Bihannic, I., Michot, L.J., Montarges-Pelletier, E., and Robert, J.L. (2009) An XPEEM study of structural cation distribution in swelling clays. I. Synthetic trioctahedral smectites. *Physics and Chemistry of Minerals*, **36**, 593–602.

Wagner, C.D. (1980) Studies of the charging insulators in ESCA. *Journal of Electron Spectroscopy and Related Phenomena*, **18**, 345–349.

Wagner, C.D., Gale, L.H., and Raymond, R.H. (1979) Two-dimensional chemical state plots: A standardized data set for use in identifying chemical states by X-ray photoelectron spectroscopy. *Analytical Chemistry*, **51**, 466–482.

Wagner, C.D., Passoja, D.E., Hillery, H.F., Kinisky, T.G., Six, H.A., Jansen, W.T., and Taylor, J.A. (1982) Auger and photoelectron line energy relationships in aluminum–oxy-oxygen and silicon–oxygen compounds. *Journal of Vacuum Science and Technology*, **21**, 933–944.

Watts, J.F. (2010) The potential for the application of X-ray photoelectron spectroscopy in forensic science. *Surface and Interface Analysis*, **42**, 358–362.

(*Received 12 April 2016; revised 5 September 2016; Ms. 1101; AE: R. Kukkadapu*)